



 Cite this: *RSC Adv.*, 2019, 9, 15381

Effect of calcination temperature, pH and catalyst loading on photodegradation efficiency of urea derived graphitic carbon nitride towards methylene blue dye solution

 Devina Rattan Paul,^a Rishabh Sharma,^a S. P. Nehra ^{*ab} and Anshu Sharma^{*c}

In this study, the photodegradation of methylene blue (MB) dye was performed using urea based graphitic carbon nitride (g-C₃N₄). Interestingly, it has been observed that the calcination temperature for the synthesis of g-C₃N₄ along with factors (pH and catalyst loading) influencing the photodegradation process, can make an impactful improvement in its photodegradation activity towards MB dye solution. The concept behind the comparatively improved photoactivity of g-C₃N₄ prepared at 550 °C was explored using various characterisation techniques like XRD, FTIR, SEM, BET and DRS. The FTIR and XRD patterns demonstrated that synthesis of g-C₃N₄ took place properly only when the calcination temperature was above 450 °C. The evolution of morphological and optical properties based on calcination temperature led to dramatically increased BET surface area and a decreased optical band gap value of g-C₃N₄ prepared at 550 °C. The effects of pH conditions and catalyst concentration on the MB dye degradation rate using optimally synthesised g-C₃N₄ are discussed. The value of the apparent rate constant was found to be 12 times more in the case of photodegradation of the MB dye using g-C₃N₄ prepared at 550 °C at optimum pH and catalyst loading conditions when compared with g-C₃N₄ prepared at 450 °C showing the lowest photoactivity potential. Further, high stability of the photocatalyst was observed for four cyclic runs of the photocatalytic reaction. Hence, g-C₃N₄ can be considered as a potential candidate for methylene blue photodegradation.

Received 21st March 2019

Accepted 11th May 2019

DOI: 10.1039/c9ra02201e

rsc.li/rsc-advances

1. Introduction

A main focus of researchers these days is establishing easier strategies to abate the complex pollutants harming the environment. In this situation every material or technology which can use solar energy as its driving source is an asset. Recently, a new method of oxidation, the “advanced oxidation processes” (AOP), has been used as an emerging eco-friendly method which leads to almost complete mineralization of pollutants.^{1,2} In regard to AOPs, the application of photocatalysis has strikingly captivated attention in recent research activities.^{3,4} A photocatalytic process relying on visible light is more convenient regarding cost aspects and is more harmonious with the environment than one using ultraviolet light. Carbon nitrides are a type of polymeric materials which can be procured from carbon materials by substituting carbon atoms with nitrogen.⁵ Among carbon nitrides, g-C₃N₄ has

been reported as substantially stable allotrope.^{6,7} It has been bestowed with generous surface properties that are vital to catalysis, such as, electron-rich properties, basic surface functionalities, bonding motif *etc.*⁸ The property of g-C₃N₄ to use visible light has made it conspicuous among other traditional metal oxides (such as TiO₂, ZnO, SnO₂) which need ultraviolet light for their functioning as photocatalyst.^{9–12} There are various prerequisites of using g-C₃N₄ as a photocatalyst. It has a band energy of 2.7 eV, due to which it is active in visible light region without any alterations.^{13,14} Additionally, for improving its photocatalytic ability band gap can be adjusted by doping or modification of nano-morphology.^{14,15} The application of g-C₃N₄ as a photoactive material has also been investigated for various reactions, including oxygen reduction, chemical sensors, humidity sensors, transesterification, photovoltaic solar cells, water splitting, catalysis of organic synthesis reactions, CO₂ activation, photodegradation of dyes, *etc.*^{13,16–21} However, its effectiveness in visible light is quite low, attributing to inadequate surface area and hindered marginal absorption of light.^{22,23} In order to improve its efficiency under visible light various modification ideologies have been implied to alter its electronic structure, such as doping with noble metals (Au, Ag, Cu, Pt, Sm) and non-metals (N, S, P), tailoring laminar structure of g-C₃N₄,

^aCenter of Excellence for Energy and Environmental Studies, Deenbandhu Chhotu Ram University of Science and Technology, Murthal 131039, India. E-mail: nehrasp@gmail.com

^bCenter for Polymers and Organic Solids, Department of Chemistry and Biochemistry, University of California at Santa Barbara, Santa Barbara, California 93106, USA

^cDepartment of Physics, Indian Institute of Technology Delhi, New Delhi 110016, India. E-mail: anshushharda@gmail.com



metallic oxide composting, copolymerization and dye sensitization.^{21,24–30} In addition to above mentioned strategies to modify g-C₃N₄, various studies showed that the calcination temperature, as well as the precursor used for synthesis greatly influence the structure, optical properties and morphology of the as-prepared sample.^{20,31,32} The above discussion gives us a tremendous opportunity to explore more of the potential of the g-C₃N₄ as promising photocatalyst towards photodegradation of dyes.

Recently many of the researchers have reported the impact of calcination temperature on g-C₃N₄ refined photoactivity. Enumerating some of results, Zhang *et al.* discussed that photoactivity of g-C₃N₄ (450 to 650 °C) towards H₂ production using thiourea got better with the increasing calcination temperature and also Mo *et al.* reported the same trend for melamine derived g-C₃N₄ for MB dye degradation.^{33,34} Gu *et al.* investigated increment in photoactivity of melamine derived g-C₃N₄ (470–570 °C) to a certain limit of calcination temperature increment for H₂ and O₂ evolution experiments and afterwards the photocatalytic activity was found to be decreasing and similar observation was also reported by Fang *et al.* for urea derived g-C₃N₄ (400–650 °C) towards rhodamine B dye.^{35,36} Contrarily, Su *et al.* reported the increase in catalytic activity with decreasing preparation temperature for urea derived g-C₃N₄ for CO₂ conversion experiment.³⁷ The above findings further suggest that the synthesis temperature and the precursor used for g-C₃N₄ acts crucially towards performance of its photoactivity. Although, Liu *et al.* has examined calcination temperature effect over the urea derived g-C₃N₄ for its structural and optical property evolution but the temperature range in which results has been reported is only up to 550 °C and in particular the effects of calcination temperature on its photocatalytic activity towards MB dye degradation in temperature range of 350 to 700 °C have not been discussed.³⁸ Therefore, we have taken the consideration for synthesizing g-C₃N₄ using urea at different calcination temperature to find out the extent of effects of calcination temperature along with factors (pH and catalyst loading) influencing photodegradation process, on the photocatalytic activity of g-C₃N₄ towards MB dye degradation. In this study, the facile preparation of g-C₃N₄ using urea at various temperatures starting from 350 °C to 700 °C has been performed. The morphological evolutions, textural structures and optical properties based on calcination temperature have been analyzed carefully. The photoactivity of g-C₃N₄ synthesized at different temperature conditions was evaluated towards MB dye solution separately for each sample. The effect of pH condition and catalyst concentration on MB dye degradation reaction rate using optimally synthesized g-C₃N₄ has been discussed. Further the recycling of the photocatalyst was done and it was reused to find out its stability as a photocatalyst. The optimally synthesized g-C₃N₄ will further allow us to find its effectiveness of photocatalytic activity towards various other organic dyes.

2. Experimental

2.1 Preparation of sample

The preparation of g-C₃N₄ was done by directly heating urea in muffle furnace adequately. 10 g urea was taken in a porcelain

covered crucible and wrapped tightly using aluminum foil paper. The calcinations of the samples were done at 350 to 750 °C at 2 °C min^{−1}, for 3 h. The schematic for plausible intermediates at different temperature range has been shown in Fig. 1.³⁸ Finally, the obtained samples were finally powdered and tagged as *t* (where *t* represents the corresponding calcination temperature) and further photocatalytic experiments followed by characterizations were performed.

2.2 Photocatalytic activity

Photoactivity evaluation of samples was done by measuring degradation of MB dye in aqueous solutions in simulated solar irradiation. Two 200 W xenon lamps fitted on the two opposite side walls of photocatalytic reactor were used as a source of simulated solar irradiation. Radiant flux was determined by power meter (194.5 W m^{−2}). For each experimental run, 10 ppm of MB aqueous dye solution containing 0.01 g of photocatalyst was taken in 250 mL of conical glass beaker. The solution was kept for stirring for 30 min in dark at room temperature to attain adsorption–desorption equilibrium. At regular time intervals 2 mL of suspensions were drawn out during the irradiation process and centrifuged immediately to separate the photocatalyst. The absorption spectrums of the drawn out samples were taken using UV-vis spectrophotometer in 450 to 800 nm wavelength range of visible spectrum. The change in major absorption peak intensity was used for evaluation of dye degradation. Photocatalytic degradation efficiency was calculated using following equation:

$$E = (1 - C/C_0) \times 100\% \text{ or } E = (1 - A/A_0) \times 100\%$$

where, *C* – concentration of the solution at time *t*, *C*₀ – adsorption/desorption equilibrium concentration of solution at time *t*₀, *A* and *A*₀ represents corresponding values.

Simplified pseudo first order kinetic model of Langmuir–Hinshewood (equation) $\ln(C_0/C_t) = k_{app}t = kKt$ (*C* – concentration of dye (mg L^{−1}), *t* – time for degradation (min), *k* – reaction rate constant (min^{−1}), *k*_{app} – apparent rate constant (min^{−1}) and *K* – adsorption coefficient of dye over catalyst particles), was utilised for estimating apparent rate constant of dye degradation process.

Further, experiments of recycling were carried for four cycles for analysing durability of photocatalytic material. After each cycle, the photocatalyst was recollected with the help of centrifugation at 6000 rpm for duration of 10 min, dried at 100 °C for 2 h and used directly for each test to analyse its reusability aspect.

2.3 Characterization

X-ray diffraction (XRD) analysis was done with Rigaku Ultima IV equipped with CuK α radiation (1.5406 Å). Fourier transform infrared spectroscopy (FTIR, PerkinElmer FRONTIER) (250–8000 cm^{−1}) analysis was carried out with standard KBr disk method. Ultraviolet visible (UV-vis) diffuse reflectance spectrum (DRS) was taken with UV-vis spectrophotometer (Shimadzu UV-2450, Japan) with standard reflectance material – BaSO₄. The



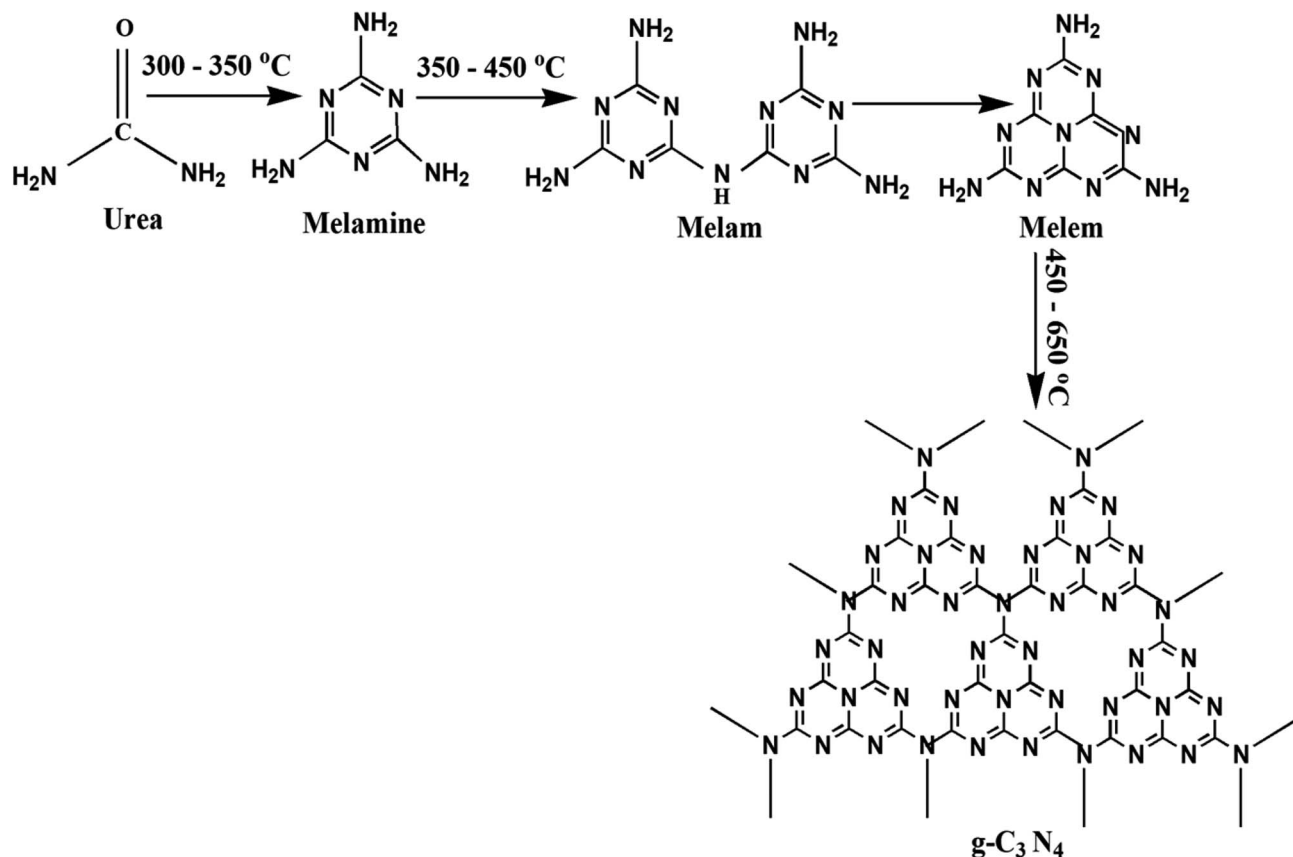


Fig. 1 Schematic for synthesis of g-C₃N₄ showing the plausible intermediates at different temperature range.

radiant flux was measured by power meter (Tenmars TM-207). Scanning electron microscope (SEM, EVO LS 10) for investigation of structural morphology. Micromeritics TriStar II 3020 nitrogen adsorption apparatus (USA) for recording Brunauer–Emmett–Teller (BET) specific surface area of samples. Degassing was performed at 180 °C before measurement. BET surface area was calculated through multipoint BET method utilising data of adsorption in range (0.05–0.2) of relative pressure (P/P_0).

3. Results and discussion

3.1 XRD analysis

In context to identify structural aspects of g-C₃N₄ synthesised at different temperatures, XRD patterns were analysed. Two major peaks of diffraction nearly 27.6° and 13.1° were spotted in the XRD patterns of g-C₃N₄ prepared at 450 °C onwards as shown in Fig. 2. The peak around 27.6° can be indexed to (002) plane resulting due to interplanar stacking of aromatic systems with an interlayer distance of $d = 0.326$ nm.^{39,40} It was observed that with rise in calcination temperature, peak (002) shifted to a higher angle (27.3° to 27.9°) depicting the corresponding change in distance of interlayer from 0.328 to 0.319 nm. This leads to a deduction that with the increasing calcination temperature the interlayer stacking order of g-C₃N₄ can be improved but heating above 550 °C will lead to a denser packing among conjugated aromatic systems resulting in formation of

more compact g-C₃N₄ with an interlayer distance of $d = 0.322$ to 0.319 nm.⁴¹ In addition, it can be clearly seen that the (002) peaks becomes more intense and narrower with increasing

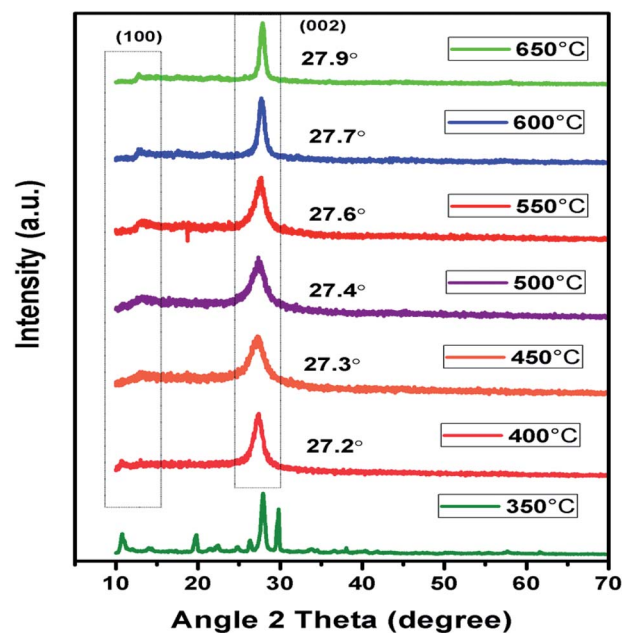


Fig. 2 XRD pattern of g-C₃N₄ prepared at different calcination temperature.



calcination temperature, indicating towards increase in crystallinity of $g\text{-C}_3\text{N}_4$ samples with increasing temperature.⁴² The other smaller peak around 13.1° could be indexed to (100) plane which corresponds to in-planar structural packing motif.^{43–45} The (100) peak was found to be intense and narrow for $g\text{-C}_3\text{N}_4$ samples at 550 to 650 $^\circ\text{C}$, indicative of higher degree of polymerisation. The broader peak for samples at 450 and 500 $^\circ\text{C}$ is indicative of low degree of polymerization of $g\text{-C}_3\text{N}_4$.⁴² It has been observed that no clear peak around 13.1° was found in the case of $g\text{-C}_3\text{N}_4$ prepared at 400 $^\circ\text{C}$ which reveals that in-planar structural packing did not take place properly below 400 $^\circ\text{C}$. Also, at 350 $^\circ\text{C}$ the obtained XRD pattern was not similar to the other samples which probably depict some intermediate of urea resulting due to low polycondensation condition.³⁴ XRD analysis revealed that the synthesis of urea derived $g\text{-C}_3\text{N}_4$ takes place at temperature higher than 450 $^\circ\text{C}$ which is further confirmed by FTIR analyses. Also, the $g\text{-C}_3\text{N}_4$ polycondensation could be optimized in the range of calcination temperature (450 to 550 $^\circ\text{C}$), but the excessive thermal heating could induce the decomposition of carbon nitride polymer. Whereas at 700 $^\circ\text{C}$ no sample was obtained which implies that $g\text{-C}_3\text{N}_4$ got fully decomposed at calcinations temperature higher than 650 $^\circ\text{C}$.

3.2 FTIR analysis

FTIR spectroscopy analysis of samples prepared at 350 to 650 $^\circ\text{C}$ as shown in Fig. 3, were performed to further analyse their chemical structure. The principal absorption band in FTIR spectra appeared in 1200 to 1650 cm^{-1} which is similar to earlier reporting. Peaks observed at 1640, 1569, 1326, 1412, and 1240 cm^{-1} correspond to stretching vibrational mode of $\text{C}=\text{C}$ and $\text{C}-\text{C}$ heterocycles.^{38,46} Intensity of these peaks was found to be increasing towards higher temperature, suggesting the increase in the degree of polymerisation. The broad band

observed between 3000 to 3400 cm^{-1} were due to $\text{N}-\text{H}$ stretching and minute adsorbed H_2O molecules.^{40,47} The intensity of the peaks in this region decreases with the corresponding increase in the synthesis temperature conveying the reduction in the number of $-\text{NH}$ or $-\text{NH}_2$ groups for the corresponding samples and increase of degree of polymerisation.³⁷ A strong peak observed at 815 cm^{-1} was designated to *s*-triazine units breathing mode.^{45,48} Whereas in case of sample prepared at 350 and 400 $^\circ\text{C}$ the formation of characteristic peaks of $g\text{-C}_3\text{N}_4$ couldn't be observed representing possibly the formation of urea intermediate and incomplete polymerisation respectively. The FTIR patterns of the samples further confirmed that the synthesis of $g\text{-C}_3\text{N}_4$ takes place at temperature higher than 450 $^\circ\text{C}$ which is in agreement with results of XRD.

3.3 SEM and TEM analysis

SEM images of samples calcined at 450 to 650 $^\circ\text{C}$ can be observed in Fig. 4(a–e). The morphology of samples obtained at 450 $^\circ\text{C}$ and 500 $^\circ\text{C}$ appeared to be consisting of lumps. Sample prepared at 550 $^\circ\text{C}$ showed the stacked layered morphology as observed from SEM and TEM images shown in Fig. 4(c and f).³² Samples prepared at 600 $^\circ\text{C}$ and 650 $^\circ\text{C}$ resulted in contraction of layered flakes of $g\text{-C}_3\text{N}_4$ suggesting the possibility of reduction of the surface area at calcination temperature above 550 $^\circ\text{C}$.

3.4 BET analysis

To understand the calcination temperature effect towards specific surface area of samples, nitrogen adsorption-desorption was utilised as presented in Fig. 5(a) together with their corresponding multipoint BET plots presented in Fig. 5(b) and Barret-Joyner-Halenda (BJH) pore size distribution curves presented in Fig. 5(c). The results for BET surface area, pore size and volume of these samples are presented in Table 1. The adsorption-desorption isotherms for all the samples under consideration showed characteristic type III curve.^{49,50} The BET specific surface areas were estimated to be 37.8 $\text{m}^2 \text{g}^{-1}$, 73.7 $\text{m}^2 \text{g}^{-1}$ and 65.6 $\text{m}^2 \text{g}^{-1}$ for $g\text{-C}_3\text{N}_4$ samples prepared at 450, 550 and 650 $^\circ\text{C}$, respectively. The most probable pore distribution in case of $g\text{-C}_3\text{N}_4$ samples obtained at 450, 550 and 650 $^\circ\text{C}$ were found to be centred at around 3.97 nm, 4.13 nm and 3.93 nm, which can be attributed to presence of mesopores. It can be observed in Fig. 5(c) that sample prepared at 450 $^\circ\text{C}$ exhibits a small peak near 4.08 nm, with rise in temperature to 550 $^\circ\text{C}$, peak at 4.08 nm grows up gradually and simultaneous peak appears at 6.91 nm and other more pronounced peak appears at 5.3 nm suggesting the increase in the number of pores during heating process in wide pore diameter distribution and volume of pore appeared as largest for the $g\text{-C}_3\text{N}_4$ prepared at 550 $^\circ\text{C}$. However, at 650 $^\circ\text{C}$ number of pores decreases. The analysis showed that calcination temperature may affect specific surface area of $g\text{-C}_3\text{N}_4$. The sample obtained at 550 $^\circ\text{C}$ had nearly 1.12 and 2 times increased surface area than samples at 650 and 450 $^\circ\text{C}$ respectively. Analysis revealed that the surface area of $g\text{-C}_3\text{N}_4$ improved effectively at 550 $^\circ\text{C}$, also showing conformity with observed morphology in SEM analysis.

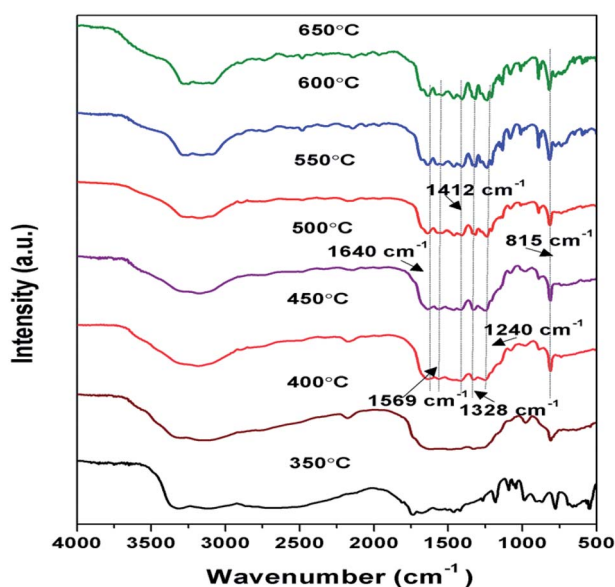


Fig. 3 FTIR pattern of $g\text{-C}_3\text{N}_4$ prepared at different calcination temperature.



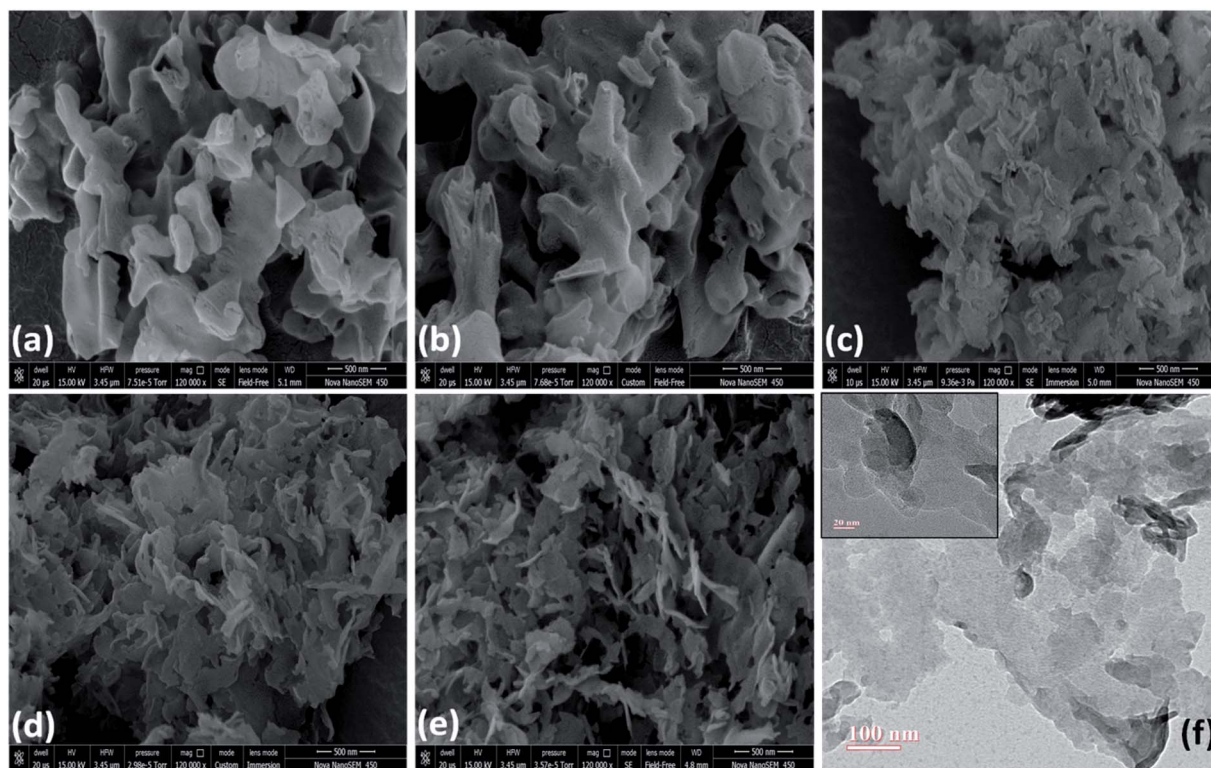


Fig. 4 SEM images of g-C₃N₄ prepared at (a) 450 °C (b) 500 °C (c) 550 °C (d) 600 °C (e) 650 °C (f) TEM image of g-C₃N₄ prepared at 550 °C.

3.5 UV-vis spectroscopic study

DRS spectra of samples calcined at different temperature were analysed as presented in Fig. 6(a), towards effect of change in calcination temperature on optical property of prepared samples. Variation in the absorption edges was observed with the change in calcination temperature. Further the band gap energy was calculated using equation: $\alpha = A(h\nu - E_g)^n/h\nu$, where α is coefficient of absorption coefficient.⁵¹ The band gap energy of samples obtained at 450, 550 and 650 °C were estimated to be 2.77, 2.72 and 2.83 eV, respectively as shown in Fig. 6(b). Firstly,

when calcination temperature was raised from 450 to 550 °C, the band gap energy showed a decreasing trend from 2.77 to 2.72 eV, this could be because of increased degree of polymerisation of g-C₃N₄, resulting in increase of π -plane conjugation degree of heptazine rings *via* N₂ atoms.⁴² When temperature was further raised to 650 °C, a blue shift in absorption edge was observed and band gap energy increased to 2.83 eV. The blue shift could be a possible result of strong quantum confinement effect and the possible reason for better photoactivity of sample obtained at 650 °C than 450 °C may be assigned to increased surface area as discussed earlier.³³ This revealed that band gap

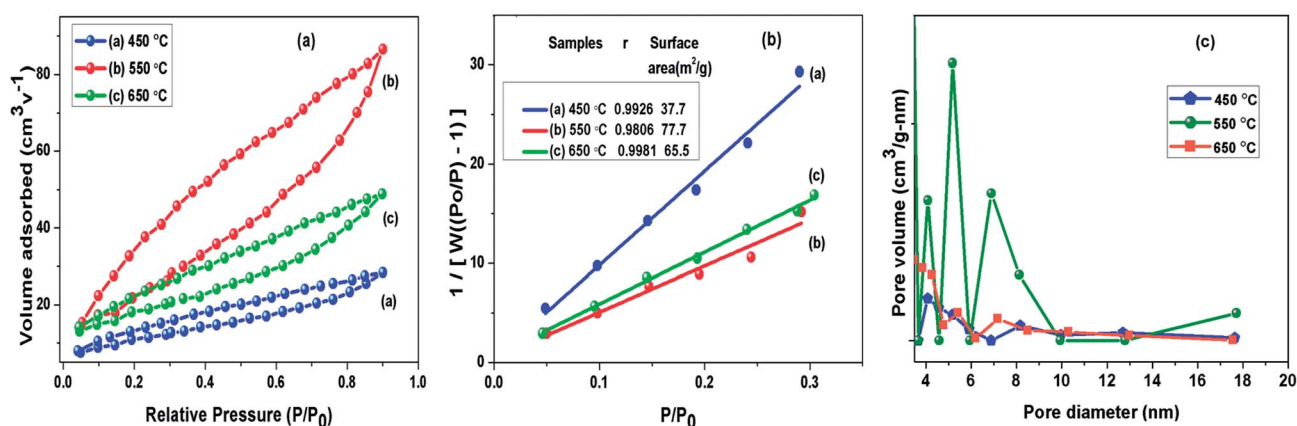


Fig. 5 (a) Nitrogen adsorption–desorption isotherm; (b) BET adsorption isotherm (c) BJH pore size distribution curve of g-C₃N₄ prepared at different calcination temperature.



Table 1 Summary of BET obtained parameters of g-C₃N₄ prepared at different calcination temperature

g-C ₃ N ₄ prepared at	S_{BET} (cm ² g ⁻¹)	Total pore vol. (cm ³ g ⁻¹)	Avg. pore radius (nm)
450 °C	37.8	0.0439	3.97
550 °C	73.7	0.1338	4.13
650 °C	65.6	0.0756	3.93

in case of g-C₃N₄ prepared at 550 °C was narrower than samples prepared at 450 and 650 °C. It can be concluded that g-C₃N₄ prepared at 550 °C had higher ability of absorbing visible light which can lead to better photoactivity in comparison to other samples in consideration.³³

3.6 Effect of calcination temperature on the photocatalytic activity

Photoactivity of g-C₃N₄ was assessed by performing photodegradation of MB dye under simulated solar irradiation separately for all the samples synthesized at different temperature conditions. Interestingly, the calcination temperature affected photodegradation activity of g-C₃N₄ noticeably towards MB dye solution. The adsorption efficiencies of g-C₃N₄ prepared at 450, 500, 550, 600 and 650 °C were about 18%, 26.8%, 34.4%, 27.7% and 21.7% for MB dye solution, respectively. The g-C₃N₄ sample calcined at 550 °C displayed highest adsorption ability and order of adsorption ability observed in case of sample prepared at 450 550 and 650 °C was found to be consistent well with their surface area as discussed earlier in this study. The degradation efficiency and the apparent rate constant measured for all the prepared samples of g-C₃N₄ at different temperatures towards MB dye for the duration of 120 min have been compared in Fig. 7(a) and (b) respectively and are represented in Table 2. Photoactivity of g-C₃N₄ was observed to be increasing corresponding to rise in calcination temperature from 450 to 550 °C

and after that photocatalytic activity was found to follow a decreasing trend from 550 to 650 °C. Sample obtained at 550 °C exhibited the maximum degradation efficiency of 62.6% in 120 min for MB dye. The results suggested that g-C₃N₄ photoactivity may be greatly refined by raising calcination temperature to some an extent and further increment of temperature may lead to decline in the photoactivity as well. The g-C₃N₄ prepared at 550 °C showed largest rate of reaction constant (*k*) of 0.0081 which is nearly 2 and 1.6 times higher than the g-C₃N₄ synthesized at 450 and 650 °C. The increased reaction rate of g-C₃N₄ calcined at 550 °C could be due to its higher efficiency of absorbing visible light which can lead to better generation of photo-generated electrons causing more efficient separation of charge and hence better photoactivity.

3.7 Optimization of photodegradation process of MB dye solution

3.7.1 pH of the solution. It was noted that the photocatalytic degradation process of pollutants got pronouncedly affected by pH of the solution. The g-C₃N₄ prepared at 550 °C was further analyzed to find the effect of pH on photodegradation process of MB dye. Initial pH of dye solution was set in the range of pH 5 to pH 11 by adjusting with dil. solution of HCl and NaOH. It was seen that when the pH value was set lesser than the normal pH in the acidic range of the MB dye solution, the fall in g-C₃N₄ photoactivity was observed where as on increasing pH value from the normal in the basic range the rise in g-C₃N₄ activity could be seen. This observation might be related to the fact that at pH value greater than 6.8 the MB dye molecules are negatively charged in alkaline medium which may result in strong adsorption of dye on the positively charged g-C₃N₄ particles because of electrostatic attraction among the two.^{40,52,53} This also implies that the formation of reactive intermediates like super oxide radicals is significantly enhanced in the alkaline medium ultimately enhancing the reaction rate. The g-C₃N₄ prepared at 550 °C showed highest

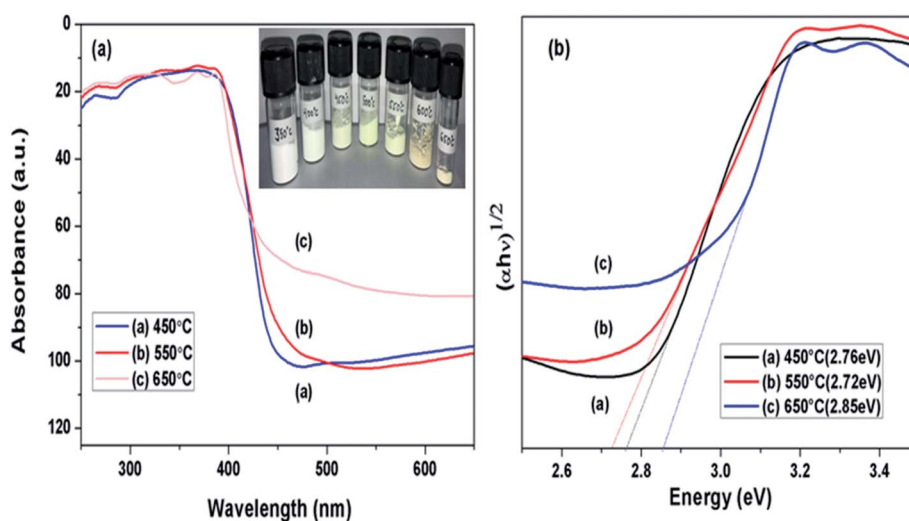


Fig. 6 (a) UV-vis diffused absorbance spectra (b) estimated band gaps of g-C₃N₄ prepared at different calcination temperature.



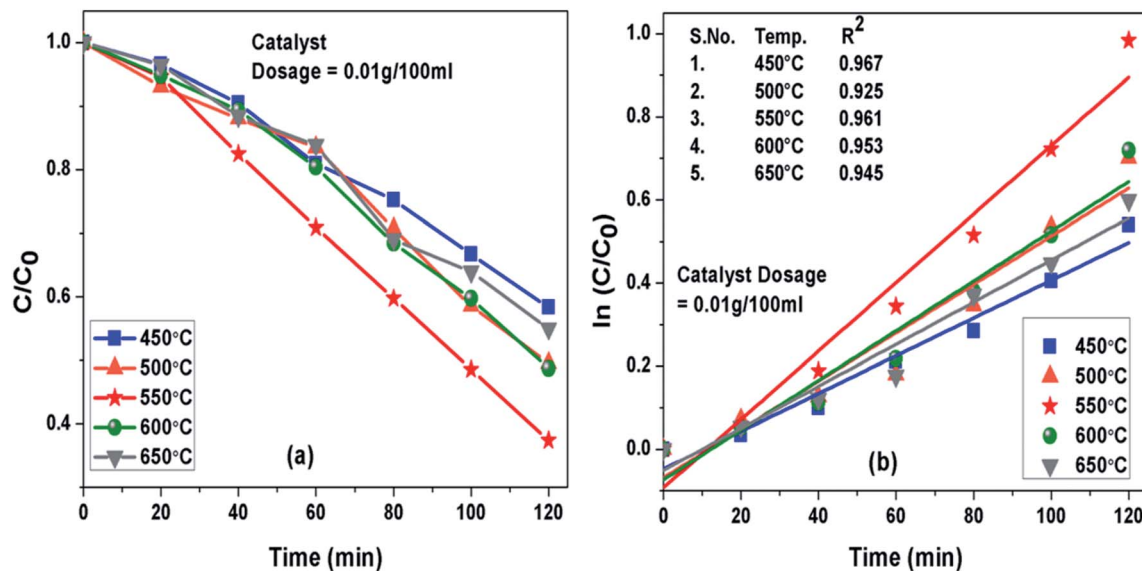


Fig. 7 (a) Comparison of photocatalytic activity of g-C₃N₄ prepared at different temperature (b) $\ln(C_0/C(t))$ for MB degradation with g-C₃N₄ prepared at different temperature as a function of simulated solar irradiation time.

Table 2 Degradation efficiency and the apparent rate constant (k) values measured for all the prepared samples of g-C₃N₄ at different temperatures

S. no.	Calcination temp. (°C)	Degradation efficiency (%)	Apparent rate constant (k) in min ⁻¹
1	450	41.6	0.0044
2	500	50.4	0.0058
3	550	62.6	0.0081
4	600	51.2	0.0059
5	650	45	0.0050

degradation efficiency of 98.7% for the MB dye solution set at pH 11 which is 1.57 times higher than the degradation efficiency at the normal pH condition. The degradation efficiency and the apparent rate constant measured for all the photocatalytic reactions for the duration of 120 min at different pH conditions are presented in Fig. 8(a) and (b) respectively and are represented in Table 3.

3.7.2 Catalyst loading. The concentration of photocatalyst (g-C₃N₄ prepared at 550 °C) was varied from 0.01 to 0.07 g per 100 mL of 10 ppm MB dye solution at pH 11 to analyse effect of catalyst concentration on photoactivity of g-C₃N₄ towards MB dye as presented in Fig. 9(a and b). It was seen that when amount of photocatalyst was increased from 0.01 g to 0.05 g the photocatalytic activity was found to be increasing which could be caused by increased active sites on catalyst surface. The further increase in catalyst amount above 0.05 g might decreased the activity due to hindrance caused to light pathway to reach dye molecules, which could be due to phenomenon of light scattering dominating at higher catalyst loading.⁵⁴ The 0.05/100 g mL⁻¹ concentration g-C₃N₄ prepared at 550 °C showed highest degradation efficiency of 100% in 60 min for

the MB dye solution set at pH 11. The percent degradation efficiency and the apparent rate constant measured for all the photocatalytic reactions for the duration of 60 min at different photocatalyst concentration are represented in Table 4.

3.8 Recycle and reusability experiment

The g-C₃N₄ sample prepared at 550 °C was checked for its stability for four cyclic runs. From Fig. 10 it can be seen that the photocatalyst showed almost same photodegradation activity towards 10 mg L⁻¹ MB dye solution for all four experiments. A minute decrease in degradation efficiency could be seen which is possibly due to loss in catalyst amount during recollection process after each run. The cycling test support the fact that g-C₃N₄ has fine stability and can be used for dye degradation application.

3.9 Factors influencing the photocatalytic activity of g-C₃N₄ towards MB dye degradation

In general, as shown in Fig. 11, when the light of suitable photon energy *i.e.* higher than band gap energy of g-C₃N₄, falls over its surface, valence band electrons on absorbing light get excited thereby moving to conduction band, generating holes in valence band. The electrons can join oxygen to generate super oxide radicals, and then superoxide radicals can lead to photo degradation of organic dye or other organic pollutants. The results of photocatalytic reaction of samples prepared at varied calcination temperature towards MB dye showed that the calcination temperature played a major role in improvement of photocatalytic ability of g-C₃N₄ sample. As observed from results photoactivity of g-C₃N₄ towards MB dye increases with rise in temperature up to 550 °C, further increment in temperature could result in decrease in activity. Some of the similar studies by Xu *et al.* and Mo *et al.* reported the highest



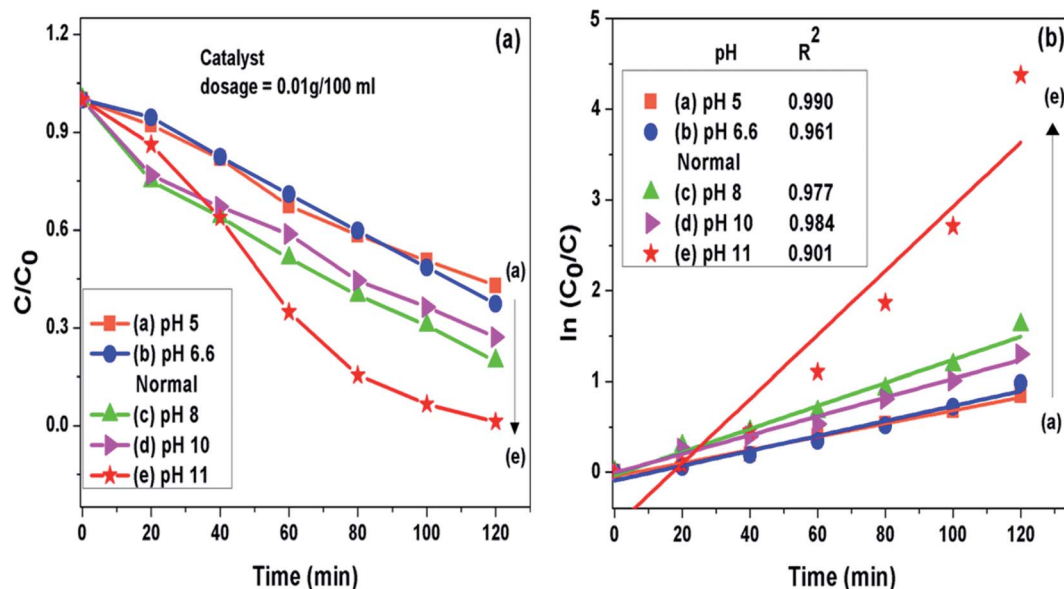


Fig. 8 (a) Comparison of photocatalytic activity of g-C₃N₄ at different pH condition (b) $\ln(C_0/C(t))$ for MB degradation with g-C₃N₄ at different pH condition as a function of simulated solar irradiation time.

Table 3 Degradation efficiency and the apparent rate constant (k) values measured for all the photocatalytic reactions for the duration of 120 min at different pH conditions

S. no.	pH value	Degradation efficiency in percent (%)	Apparent rate constant (k) in min ⁻¹
1	pH 5	57	0.00735
2	pH 6.6 (normal)	62.6	0.00811
3	pH 8	72.7	0.01022
4	pH 10	80.2	0.01265
5	pH 11	98.7	0.03398

activity for sample prepared at 600 and 650 °C respectively, in range of 450 to 650 °C.^{34,42} The variation in the result could be possibly based on the factors like the duration for which calcination was being carried out and precursor used for synthesising g-C₃N₄ which can probably affect the degree of polymerisation. The XRD analysis revealed that the calcination temperature had a huge impact on polymerization process of prepared g-C₃N₄ samples. Increasing temperature to a limit can result in an improved structure with appropriate interlayer distance of aromatic systems. Whereas the higher temperature condition can induce the bulking as well as thermal decomposition of the polymeric material, as can also be observed in the inset of Fig. 6(a) that the amount of sample obtained got reduced with the rising calcination temperature and striking decrement in amount was observed for sample obtained at 650 °C. In case of g-C₃N₄, protonation depends primarily on degree of polymerization, but also get influenced by degree of condensation. In case of g-C₃N₄, “underpolymerization” (as for sample obtained at 450 °C), leads to incomplete coupling of heptazine, resulting in excessive hydrogen-passivating N3c' nitrogen sites, thereby hindering activity. The

“overpolymerization” (as in case of sample obtained at 650 °C), the structure of g-C₃N₄ becomes excessively condensed into deformed multilayered crystals having reduced surface area, resulting in reduced density of active sites, and thus adversely affecting photocatalytic ability.⁴⁰ Moreover, sp² planar geometry also gets contorted because of buckling, thus could lead to trapping states of charge at nitrogen sites and therefore decreased activity.⁴⁰ As revealed from BET analysis, the increased surface area for g-C₃N₄ prepared at 550 °C as a consequence of morphological evolution caused due to appropriate calcination temperature, which not only can lead to the formation of surface active sites for reaction but can also facilitate the separation of charge carrier because exfoliated and altered structures can reduce distance of migration for photo-generated charge carriers and thus can decrease the probability of charge recombination.³² From DRS analysis it was found that the g-C₃N₄ prepared at 550 °C also showed better ability for the absorption of light and thus may result in enhancement of photoactivity. The calculated value of reaction rate constant in case of g-C₃N₄ at 550 °C was found to be 2 to 1.5 times higher than g-C₃N₄ prepared at other temperature. Also, the factors like pH and catalyst loading resulted in the observable increment of nearly 6.6 times in the value of rate of reaction constant of g-C₃N₄ prepared at 550 °C which could be due to enhanced formation of reactive intermediates and increased active sites on catalyst surface respectively. In addition, value of reaction rate constant for MB dye degradation of g-C₃N₄ obtained at 550 °C (catalyst conc. of 0.1 g L⁻¹) was found to be 1.35 times higher when compared with the value reported by Mo *et al.* for melamine derived g-C₃N₄ at 650 °C (the optimum temperature condition, catalyst conc. 0.5 g L⁻¹).³⁴ The comparison in reaction rate constant values suggest that urea might be considered as a better precursor option for preparing g-C₃N₄ over melamine and it can be further supported by the fact that BET specific



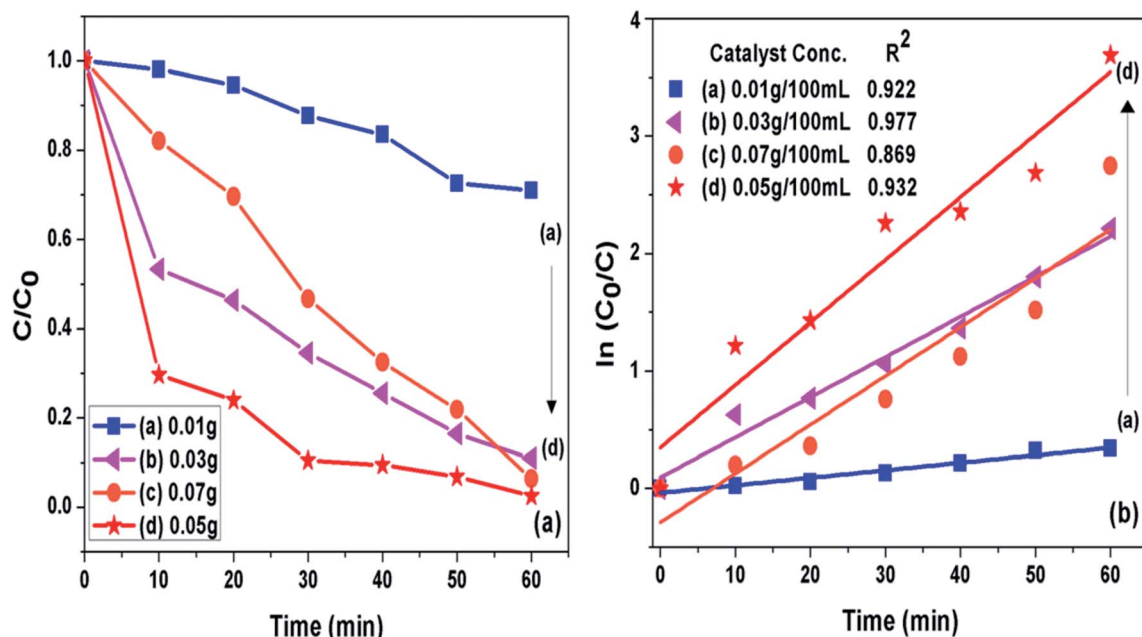


Fig. 9 (a) Comparison of photocatalytic activity of $g-C_3N_4$ at different catalyst concentration (b) $\ln(C_0/C(t))$ for MB degradation with $g-C_3N_4$ at different catalyst concentration as a function of simulated solar irradiation time.

Table 4 Degradation efficiency and the apparent rate constant (k) values measured for all the photocatalytic reactions for the duration of 60 min at different photocatalyst concentration

S. no.	Catalyst conc. (g/100 mL of 10 ppm MB dye solution at pH 11)	Degradation efficiency in percent (%)	Apparent rate constant (k) in min^{-1}
1	0.01	60	0.01653
2	0.03	89	0.03422
3	0.07	93	0.04156
4	0.05	100	0.05331

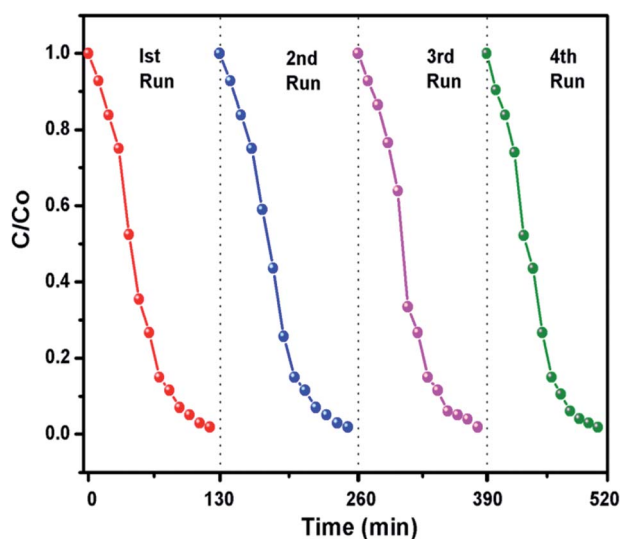


Fig. 10 Recyclability experiment of the photocatalytic degradation of dyes using $g-C_3N_4$ prepared at 550 °C.

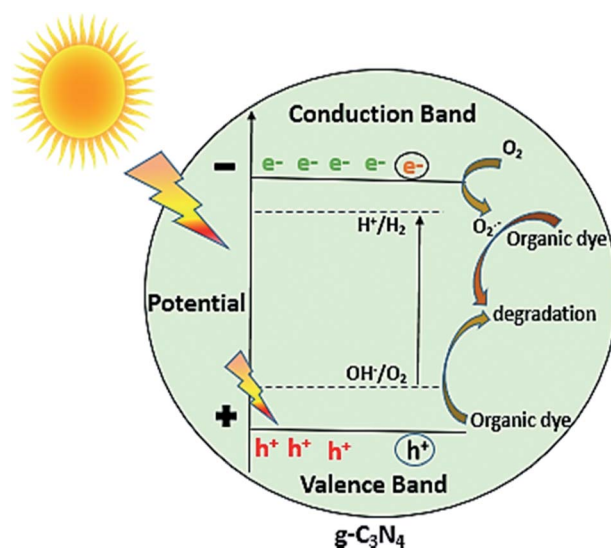


Fig. 11 Photocatalytic mechanism of $g-C_3N_4$.



surface area and calculated band gap was found to be better for optimally synthesised urea derived g-C₃N₄ that is 73.7 m² g⁻¹ and 2.72 eV where as for melamine derived g-C₃N₄ was 46.8 m² g⁻¹ and 2.74 eV respectively.³⁴ The above discussion can lead to a conclusion that improved activity of g-C₃N₄ prepared at 550 °C or the observed trend between activities with calcination temperature has found to be clearly based on the evolutions related to optical, structural and morphological properties of g-C₃N₄ brought due to different temperature conditions, choice of precursor and other optimization factors like pH and catalyst concentration of MB dye solution.

3.10. Conclusion

In summary, the g-C₃N₄ was synthesised using urea at different calcination temperature. It was noted that the photocatalytic performance of g-C₃N₄ towards MB dye solution firstly got better with increasing calcination temperature up to 550 °C and further increment of temperature leads to decrease in the photoactivity of g-C₃N₄. XRD, FTIR, SEM, BET and DRS analysis revealed that the highest photoactivity performance of g-C₃N₄ prepared at 550 °C may be due to the appropriate degree of polymerisation and condensation, increased surface area resulting in enhanced light absorption ability and more number of active sites. Factors like pH of solution and catalyst loading also affected effectively the photodegradation process of MB dye solution. The g-C₃N₄ prepared at 550 °C also showed the good stability even after four cyclic runs. The study inferences that the optimally synthesised g-C₃N₄ along with various factors influencing photodegradation process can be used as a potential material for degrading MB dye and can be explored further for its photocatalytic performance towards various other organic pollutants.

Conflicts of interest

There are no conflicts to declare.

Acknowledgements

DRP thanks Deenbandhu Chhotu Ram University of Science and Technology for providing financial support under the University Doctoral Research Fellowship scheme. AS acknowledges Indo-German Science and Technology Centre and Department of Science and Technology, Govt. of India for providing Max Planck India Mobility Grant award and Women Scientists Scheme-A grant respectively. SPN thanks Indo-US Science and Technology Forum and Department of Science and Technology, Govt. of India for providing research opportunity under IUSSTF BASE Fellowships 2018/2.

References

- 1 R. Andreozzi, *Catal. Today*, 1999, **53**, 51–59.
- 2 M. A. Quiroz, E. R. Bandala and C. A. Martinez-Huitle, Advanced Oxidation Processes (AOPs) for Removal of

- Pesticides from Aqueous Media, *Pesticides - Formulations, Effects, Fate*, ed. M. Stoytcheva, 2011.
- 3 V. Binas, D. Venieri, D. Kotzias and G. Kiriakidis, *J. Materiomics*, 2017, **3**, 3–16.
- 4 A. Ibhaddon and P. Fitzpatrick, *Catalysts*, 2013, **3**, 189–218.
- 5 J. Liu, H. Wang and M. Antonietti, *Chem. Soc. Rev.*, 2016, **45**, 2308–2326.
- 6 T. S. Miller, A. B. Jorge, T. M. Suter, A. Sella, F. Corà and P. F. McMillan, *Phys. Chem. Chem. Phys.*, 2017, **19**, 15613–15638.
- 7 J. Zhu, P. Xiao, H. Li and S. A. C. Carabineiro, *ACS Appl. Mater. Interfaces*, 2014, **6**, 16449–16465.
- 8 A. Thomas, A. Fischer, F. Goettmann, M. Antonietti, J. O. Müller, R. Schlögl and J. M. Carlsson, *J. Mater. Chem.*, 2008, **18**, 4893.
- 9 A. L. Linsebigler, G. Lu and J. T. Yates, *Chem. Rev.*, 1995, **95**, 735–758.
- 10 M. Gaidi, A. Hajjaji, M. A. El Khakani, B. Chenevier, M. Labeau and B. Bessaïs, *Jpn. J. Appl. Phys.*, 2009, **48**, 072501.
- 11 J. Ben Naceur, M. Gaidi, F. Bousbih, R. Mechiakh and R. Chtourou, *Curr. Appl. Phys.*, 2012, **12**, 422–428.
- 12 L. Zhou, H. Zhang, H. Sun, S. Liu, M. O. Tade, S. Wang and W. Jin, *Catal. Sci. Technol.*, 2016, **6**, 7002–7023.
- 13 X. Wang, K. Maeda, A. Thomas, K. Takanabe, G. Xin, J. M. Carlsson, K. Domen and M. Antonietti, *Nat. Mater.*, 2008, **8**, 76–80.
- 14 X. Wang, S. Blechert and M. Antonietti, *ACS Catal.*, 2012, **2**, 1596–1606.
- 15 J. Zhu, Y. Wei, W. Chen, Z. Zhao and A. Thomas, *Chem. Commun.*, 2010, **46**, 6965.
- 16 R. Malik, V. K. Tomer, V. Chaudhary, M. S. Dahiya, A. Sharma, S. P. Nehra, S. Duhan and K. Kailasam, *J. Mater. Chem. A*, 2017, **5**, 14134–14143.
- 17 J. Cheng, Z. Hu, K. Lv, X. Wu, Q. Li, Y. Li, X. Li and J. Sun, *Appl. Catal., B*, 2018, **232**, 330–339.
- 18 J. Cheng, Z. Hu, Q. Li, X. Li, S. Fang, X. Wu, M. Li, Y. Ding, B. Liu, C. Yang, L. Wen, Y. Liu and K. Lv, *Appl. Catal., B*, 2018, **245**, 197–206.
- 19 J. C. Wang, H. C. Yao, Z. Y. Fan, L. Zhang, J. S. Wang, S. Q. Zang and Z. J. Li, *ACS Appl. Mater. Interfaces*, 2016, **8**, 3765–3775.
- 20 P. Niu, L. Zhang, G. Liu and H. M. Cheng, *Adv. Funct. Mater.*, 2012, **22**, 4763–4770.
- 21 D. R. Paul, R. Sharma, P. Panchal, R. Malik, A. Sharma, V. K. Tomer and S. P. Nehra, *J. Nanosci. Nanotechnol.*, 2019, **19**, 1–8.
- 22 H. Xu, Y. Song, Y. Song, J. Zhu, T. Zhu, C. Liu, D. Zhao, Q. Zhang and H. Li, *RSC Adv.*, 2014, **4**, 34539.
- 23 M. Wu, J. M. Yan, X. W. Zhang, M. Zhao and Q. Jiang, *J. Mater. Chem. A*, 2015, **3**, 15710–15714.
- 24 N. Cheng, J. Tian, Q. Liu, C. Ge, A. H. Qusti, A. M. Asiri, A. O. Al-Youbi and X. Sun, *ACS Appl. Mater. Interfaces*, 2013, **5**, 6815–6819.
- 25 S. Le, T. Jiang, Q. Zhao, X. Liu, Y. Li, B. Fang and M. Gong, *RSC Adv.*, 2016, **6**, 38811–38819.



- 26 B. Liu, L. Ye, R. Wang, J. Yang, Y. Zhang, R. Guan, L. Tian and X. Chen, *ACS Appl. Mater. Interfaces*, 2018, **10**, 4001–4009.
- 27 J. Thomas, K. S. Ambili and S. Radhika, *Catal. Today*, 2018, **310**, 11–18.
- 28 Z. Yang, Z. Yao, G. Li, G. Fang, H. Nie, Z. Liu, X. Zhou, X. Chen and S. Huang, *ACS Nano*, 2011, **6**, 205–211.
- 29 W. J. Ong, L. L. Tan, S. P. Chai and S. T. Yong, *Dalton Trans.*, 2015, **44**, 1249–1257.
- 30 J. Fang, H. Fan, M. Li and C. Long, *J. Mater. Chem. A*, 2015, **3**, 13819–13826.
- 31 S. Wang, C. Li, T. Wang, P. Zhang, A. Li and J. Gong, *J. Mater. Chem. A*, 2014, **2**, 2885.
- 32 H. B. Fang, X. H. Zhang, J. Wu, N. Li, Y. Z. Zheng and X. Tao, *Appl. Catal., B*, 2018, **225**, 397–405.
- 33 G. Zhang, J. Zhang, M. Zhang and X. Wang, *J. Mater. Chem.*, 2012, **22**, 8083.
- 34 Z. Mo, X. She, Y. Li, L. Liu, L. Huang, Z. Chen, Q. Zhang, H. Xu and H. Li, *RSC Adv.*, 2015, **5**, 101552–101562.
- 35 Q. Gu, Z. Gao, H. Zhao, Z. Lou, Y. Liao and C. Xue, *RSC Adv.*, 2015, **5**, 49317–49325.
- 36 H. B. Fang, Y. Luo, Y. Z. Zheng, W. Ma and X. Tao, *Ind. Eng. Chem. Res.*, 2016, **55**, 4506–4514.
- 37 Q. Su, J. Sun, J. Wang, Z. Yang, W. Cheng and S. Zhang, *Catal. Sci. Technol.*, 2014, **4**, 1556.
- 38 J. Liu, T. Zhang, Z. Wang, G. Dawson and W. Chen, *J. Mater. Chem.*, 2011, **21**, 14398.
- 39 Y. Zhang, J. Liu, G. Wu and W. Chen, *Nanoscale*, 2012, 5300.
- 40 D. J. Martin, K. Qiu, S. A. Shevlin, A. D. Handoko, X. Chen, Z. Guo and J. Tang, *Angew. Chem., Int. Ed.*, 2014, **12**, 9394–9399.
- 41 P. Niu, G. Liu and H. M. Cheng, *J. Phys. Chem. C*, 2012, **116**, 11013–11018.
- 42 J. Xu, Y. Li, S. Peng, G. Lu and S. Li, *Phys. Chem. Chem. Phys.*, 2013, **15**, 7657.
- 43 F. Dong, L. Wu, Y. Sun, M. Fu, Z. Wu and S. C. Lee, *J. Mater. Chem.*, 2011, **21**, 15171.
- 44 Y. Yang, Q. Zhang, R. Zhang, T. Ran, W. Wan and Y. Zhou, *Front. Chem.*, 2018, **6**, 156.
- 45 D. Das, D. Banerjee, B. Das, N. S. Das and K. K. Chattopadhyay, *Mater. Res. Bull.*, 2017, **89**, 170–179.
- 46 Y. Li, K. Lv, W. Ho, Z. Zhao and Y. Huang, *Chinese J. Catal.*, 2017, **38**(2), 321–329.
- 47 J. L. Zimmerman, R. Williams, V. N. Khabashesku and J. L. Margrave, *Nano Lett.*, 2001, **1**, 731–734.
- 48 Q. Xiang, J. Yu and M. Jaroniec, *J. Phys. Chem. C*, 2011, **115**, 7355–7363.
- 49 A. Bahuguna, A. Kumar, S. Kumar, T. Chhabra and V. Krishnan, *ChemCatChem*, 2018, **10**, 3121–3132.
- 50 A. Bahuguna, P. Choudhary, T. Chhabra and V. Krishnan, *ACS Omega*, 2018, **3**(9), 12163–12178.
- 51 R. S. Mane, S. J. Roh, O. S. Joo, C. D. Lokhande and S. H. Han, *Electrochim. Acta*, 2005, **50**, 2453–2459.
- 52 A. F. Alkaim, A. M. Aljeboree, N. A. Alrazaq, S. J. Baqir, F. H. Hussein and A. J. Lilo, *Asian J. Chem.*, 2014, **26**, 8445–8448.
- 53 L. Heymann, B. Schiller, H. Noei, A. Stierle and C. Klinke, *ACS Omega*, 2018, **3**, 3892–3900.
- 54 S. Ahmed, M. G. Rasul, W. N. Martens, R. Brown and M. A. Hashib, *Water, Air, Soil Pollut.*, 2010, **215**, 3–29.

